Perfectly Matched Layer Media for an Unconditionally Stable Three-Dimensional ADI-FDTD Method

Gang Liu and Stephen D. Gedney

***Abstract*—A split field perfectly matched layer (PML) medium is introduced for the three-dimensional (3–D) alternating direction implicit (ADI) formulation of the finite–difference time-domain (FDTD) method. It is demonstrated that the ADI-FDTD method remains unconditionally stable with the inclusion of the PML. The effectiveness of the absorbing medium as a function of the time step is also demonstrated.**

***Index Terms*—Alternating direction implicit (ADI) method, FDTD method, perfectly matched layer (PML).**

I. Introduction

RECENTLY, an unconditionally stable three-dimensional (3-D) alternating direction implicit (ADI) scheme was introduced for the finite–difference time-domain (FDTD) method [1]. The successful implementation of this scheme has the potential to significantly impact the application of the FDTD method to problems where very fine meshing is necessary over large geometric areas. For the ADI-FDTD method to have a true impact on the field of computational electromagnetics an accurate and efficient absorbing boundary condition must be developed to emulate electromagnetic interaction in an unbounded space. The perfectly matched layer (PML) absorbing medium is an ideal candidate for the ADI-FDTD grid termination due to its broad band absorption characteristics and application to general media [2]–[4]. Furthermore, it does not corrupt the unconditional stability of the ADI-FDTD scheme.

In this letter, a split field PML based on Berenger's original formulation [2] is employed within the ADI-FDTD formulation. It is shown that the method remains unconditionally stable. The accuracy of the PML as a function of the time step is also demonstrated through example.

II. Formulations

The ADI-FDTD formulation derived herein is based on Berenger's original split field representation of Maxwell's equations [2]–[4]. For example, consider the x-projection of Ampere's law

$$\left(\varepsilon_0\varepsilon_r\frac{\partial}{\partial t}+\sigma_y\varepsilon_r\right)E_{xy}=\frac{\partial}{\partial y}\left(H_{zx}+H_{zy}\right) \tag{1a}$$

$$\left(\varepsilon_0\varepsilon_r\frac{\partial}{\partial t}+\sigma_z\varepsilon_r\right)E_{xz}=-\frac{\partial}{\partial z}\left(H_{yx}+H_{yz}\right) \tag{1b}$$

and the z-projection of Faraday's law

$$\left(\mu_0\mu_r\frac{\partial}{\partial t}+\sigma_x\eta_0^2\mu_r\right)H_{zx}=-\frac{\partial}{\partial x}\left(E_{yx}+E_{yz}\right) \tag{2a}$$

$$\left(\mu_0\mu_r\frac{\partial}{\partial t}+\sigma_y\eta_0^2\mu_r\right)H_{zy}=\frac{\partial}{\partial y}\left(E_{xy}+E_{xz}\right) \tag{2b}$$

where η_o is the free-space wave impedance.

The 3-D space is discretized using a staggered grid, as for the standard Yee-scheme. Then, following the ADI method introduced by [1], the discrete forms of (1a) and (1b) at time-step $n+1/2$ are expressed as

$$\begin{aligned}e^{n+(1/2)}_{xy_{i+(1/2),\,j,\,k}}=&\,\alpha_{y_j}e^{n}_{xy_{i+(1/2),\,j,\,k}}+\frac{\Delta x}{\Delta y\Delta z}\frac{\beta_{y_j}}{\varepsilon_{r_{i+(1/2),\,j,\,k}}}\\&\cdot\Big[h^{n+(1/2)}_{zx_{i+(1/2),\,j+(1/2),\,k}}-h^{n+(1/2)}_{zx_{i+(1/2),\,j-(1/2),\,k}}\\&+h^{n+(1/2)}_{zy_{i+(1/2),\,j+(1/2),\,k}}-h^{n+(1/2)}_{zy_{i+(1/2),\,j-(1/2),\,k}}\Big]\end{aligned} \tag{3a}$$

$$\begin{aligned}e^{n+(1/2)}_{xz_{i+(1/2),\,j,\,k}}=&\,\alpha_{z_k}e^{n}_{xz_{i+(1/2),\,j,\,k}}+\frac{\Delta x}{\Delta y\Delta z}\frac{\beta_{z_k}}{\varepsilon_{r_{i+(1/2),\,j,\,k}}}\\&\cdot\Big[h^{n}_{yx_{i+(1/2),\,j,\,k-(1/2)}}-h^{n}_{yx_{i+(1/2),\,j,\,k+(1/2)}}\\&+h^{n}_{yz_{i+(1/2),\,j,\,k-(1/2)}}-h^{n}_{yz_{i+(1/2),\,j,\,k+(1/2)}}\Big]\end{aligned} \tag{3b}$$

and discrete forms of (2a) and (2b) at time-step $n+1/2$ are expressed as

$$\begin{aligned}h^{n+(1/2)}_{zx_{i+(1/2),\,j+(1/2),\,k}}=&\,\alpha_{x_{i+(1/2)}}h^{n}_{zx_{i+(1/2),\,j+(1/2),\,k}}\\&+\frac{\Delta z}{\Delta x\Delta y}\frac{\beta_{x_{i+(1/2)}}}{\mu_{r_{i+(1/2),\,j+(1/2),\,k}}}\\&\cdot\Big[e^{n}_{yx_{i,\,j+(1/2),\,k}}-e^{n}_{yx_{i+1,\,j+(1/2),\,k}}\\&+e^{n}_{yz_{i,\,j+(1/2),\,k}}-e^{n}_{yz_{i+1,\,j+(1/2),\,k}}\Big]\end{aligned} \tag{4a}$$

$$\begin{aligned}h^{n+(1/2)}_{zy_{i+(1/2),\,j+(1/2),\,k}}=&\,\alpha_{y_{j+(1/2)}}h^{n}_{zy_{i+(1/2),\,j+(1/2),\,k}}\\&+\frac{\Delta z}{\Delta x\Delta y}\frac{\beta_{y_{j+(1/2)}}}{\mu_{r_{i+(1/2),\,j+(1/2),\,k}}}\\&\cdot\Big[e^{n+(1/2)}_{xy_{i+(1/2),\,j+1,\,k}}-e^{n+(1/2)}_{xy_{i+(1/2),\,j,\,k}}\\&+e^{n+(1/2)}_{xz_{i+(1/2),\,j+1,\,k}}-e^{n+(1/2)}_{xz_{i+(1/2),\,j,\,k}}\Big]\end{aligned} \tag{4b}$$

Manuscript received March 30, 2000; revised May 16, 2000. This work was supported by the National Science Foundation under Grants ECS-9624628 and CDA-9502645.

The authors are with the Department of Electrical Engineering, University of Kentucky, Lexington, KY 40506-0046 USA (e-mail: gedney@engr.uky.edu).

Publisher Item Identifier S 1051-8207(00)06505-3.

where

$$\alpha_{s_\ell} = \frac{\left(\frac{2}{c_0\Delta t} - \frac{\sigma_{s_\ell}\eta_0}{2}\right)}{\left(\frac{2}{c_0\Delta t} + \frac{\sigma_{s_\ell}\eta_0}{2}\right)}, \quad \beta_{s_\ell} = \left[\left(\frac{2}{c_0\Delta t} + \frac{\sigma_{s_\ell}\eta_0}{2}\right)\right]^{-1} \tag{5}$$

where c_o is the speed of light in free space, and $s = x$, y, or z and $\ell = i$, j, or k. Note that the discrete time differencing is assumed over an interval of $\Delta t/2$. The fields have also been normalized using

$$\left.\begin{aligned} e_{uv} &= E_{uv}\Delta u/\sqrt{\eta_o} \\ h_{uv} &= H_{uv}\Delta u\sqrt{\eta_o} \end{aligned}\right\} \quad u = x,\, y,\, z;\; v = x,\, y,\, z. \tag{6}$$

The remaining projections of Ampere's and Faraday's laws are similarly discretized.

A set of implicit equations can now be formulated. To this end, and (4b) are combined with (3a), leading to

$$\begin{aligned} &-\frac{1}{\Delta y^2}\frac{\beta_{y_j}\beta_{y_{j+(1/2)}}}{\varepsilon_{r_{i+(1/2),\,j,\,k}}\mu_{r_{i+(1/2),\,j+(1/2),\,k}}} e^{n+1/2}_{xy_{i+(1/2),\,j+1,\,k}} \\ &\quad + \left[1 + \frac{1}{\Delta y^2}\frac{\beta_{y_j}}{\varepsilon_{r_{i+(1/2),\,j,\,k}}} \right. \\ &\qquad \left. \cdot \left(\frac{\beta_{y_{j+(1/2)}}}{\mu_{r_{i+(1/2),\,j+(1/2),\,k}}} + \frac{\beta_{y_{j-(1/2)}}}{\mu_{r_{i+(1/2),\,j-(1/2),\,k}}}\right)\right] e^{n+1/2}_{xy_{i+(1/2),\,j,\,k}} \\ &\quad - \frac{1}{\Delta y^2}\frac{\beta_{y_j}\beta_{y_{j-(1/2)}}}{\varepsilon_{r_{i+(1/2),\,j,\,k}}\mu_{r_{i+(1/2),\,j-(1/2),\,k}}} e^{n+1/2}_{xy_{i+(1/2),\,j-1,\,k}} \\ &\quad = \alpha_{y_j} e^{n}_{xy_{i+(1/2),\,j,\,k}} + \frac{\Delta x}{\Delta y\Delta z}\frac{\beta_{y_j}}{\varepsilon_{r_{i+(1/2),\,j,\,k}}}(\xi_j - \xi_{j-1} + \chi) \end{aligned} \tag{7}$$

where

$$\begin{aligned} \xi_j &= \alpha_{x_{i+(1/2)}} h^n_{zx_{i+(1/2),\,j+(1/2),\,k}} + \frac{\Delta z}{\Delta x\Delta y}\frac{\beta_{x_{i+(1/2)}}}{\mu_{r_{i+(1/2),\,j+(1/2),\,k}}} \\ &\quad \cdot \left[e^n_{yx_{i,\,j+(1/2),\,k}} - e^n_{yx_{i+1,\,j+(1/2),\,k}} + e^n_{yz_{i,\,j+(1/2),\,k}} \right. \\ &\qquad \left. - e^n_{yz_{i+1,\,j+(1/2),\,k}}\right] \end{aligned} \tag{8a}$$

$$\begin{aligned} \chi &= \left[\alpha_{y_{j+(1/2)}} h^n_{zy_{i+(1/2),\,j+(1/2),\,k}} \right. \\ &\qquad \left. - \alpha_{y_{j-(1/2)}} h^n_{zy_{i+(1/2),\,j-(1/2),\,k}}\right] + \frac{\Delta z}{\Delta x\Delta y} \\ &\quad \cdot \left[\frac{\beta_{y_{j+(1/2)}}}{\mu_{r_{i+(1/2),\,j+(1/2),\,k}}}(\zeta_{j+1} - \zeta_j) \right. \\ &\qquad \left. + \frac{\beta_{y_{j-(1/2)}}}{\mu_{r_{i+(1/2),\,j-(1/2),\,k}}}(\zeta_{j-1} - \zeta_j)\right] \end{aligned} \tag{8b}$$

$$\begin{aligned} \zeta_j &= \alpha_{z_k} e^n_{xz_{i+(1/2),\,j,\,k}} + \frac{\Delta x}{\Delta y\Delta z}\frac{\beta_{z_k}}{\varepsilon_{r_{i+(1/2),\,j,\,k}}} \\ &\quad \cdot \left[h^n_{yx_{i+(1/2),\,j,\,k-(1/2)}} - h^n_{yx_{i+(1/2),\,j,\,k+(1/2)}} \right. \\ &\qquad \left. + h^n_{yz_{i+(1/2),\,j,\,k-(1/2)}} - h^n_{yz_{i+(1/2),\,j,\,k+(1/2)}}\right]. \end{aligned} \tag{8c}$$

Equation (7) combined with (8a)–(8c) provides the implicit update expression for the electric field component e_{xy} at the $(n + (1/2))$ time-step. The implicit equation requires the solution of a tri-diagonal matrix that couples e_{xy} along the j-axis only. This is efficiently solved in $O(N_y)$ operations [5], where N_y is the number of cells along the y-direction. Similar procedures can be used for other field components at the $(n + 1/2)$ and $(n + 1)$ time-step, respectively.

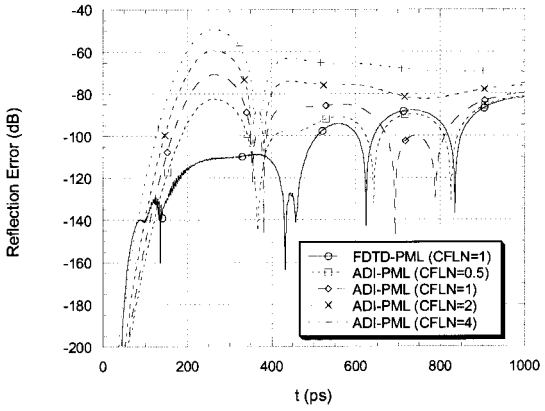

Fig. 1. Relative error at point A as a function of time for different CFL numbers.

Following a Von Neumann analysis by assuming a homogeneous PML medium, it can be shown that this scheme is unconditionally stable. Due to space limitations, this is not done here and is left to a future publication.

III. Numerical Results

To illustrate the PML termination of the ADI-FDTD lattice, a simulation of a small electric current source radiating in free-space was studied. To this end, a uniform mesh with cell spacing $\Delta x = \Delta y = \Delta z = 1$ mm and lattice dimension of $42 \times 42 \times 42$ was used. PML layers that were ten cells thick terminated all six sides of the lattice. Within the PML, the conductivity was scaled using polynomial scaling [2], [4]

$$\sigma_s(s) = \frac{\sigma_{s_{\max}}|s - s_0|^m}{d^m}, \quad s = x,\, y,\, z \tag{9}$$

where s_0 is the interface, d is the depth of the PML, and m is the order of the polynomial.

A choice for $\sigma_{s_{\max}}$ that will minimize reflection is expressed as [4]

$$\sigma_{s_{\max}} = \sigma_{opt} \approx \frac{(m+1)}{150\pi\Delta s} \tag{10}$$

where Δs is the grid spacing along the normal axis.

The reflection error due to the PML was studied by exciting a small electric dipole at the center of the grid. The time dependence of the source was a differentiated Gaussian pulse with a half-bandwidth of 3.175 GHz (note that at 3.175 GHz, the ratio of the wavelength λ_o to the grid cell size $\Delta s = 1$ mm is $\lambda_o/\Delta s = 94.5$). The reflection error was computed at two points in the grid. Point A corresponds to an electric field co-polarized with the source one cell from the PML interface and in the same plane as the source. Point B corresponds to an electric field co-polarized with the source one cell diagonally from a corner of the PML interface. A reference solution based on an extended lattice was computed for each CFLN in order to isolate the error due to the PML from grid dispersion error. The relative error was then computed as $|E_{\rm PML}(t) - E_{ref}(t)|/|E_{\max}|$,

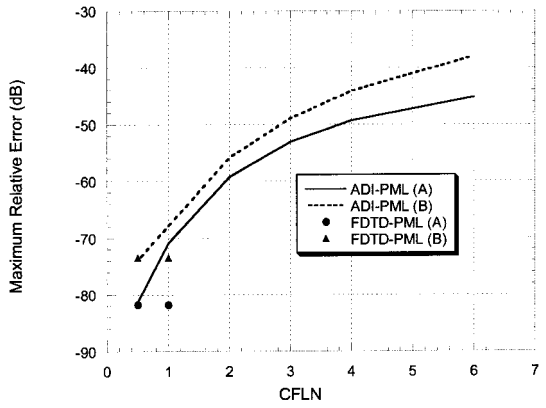

Fig. 2. Maximum relative error of the ADI-PML and Berenger's PML as the function of the CFLN.

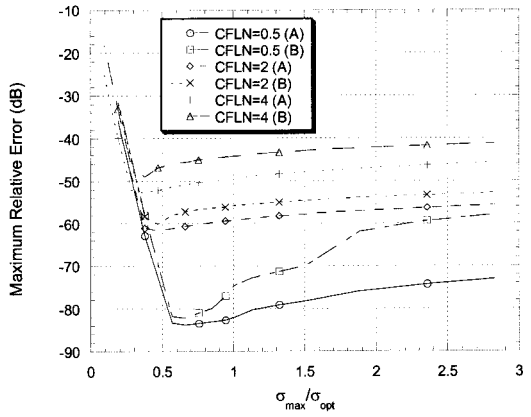

Fig. 3. Maximum relative error versus $\sigma_{\max}/\sigma_{opt}$ over a 1000 ps observation period for various CFLN's.

where $E_{\max}$ is the maximum value of the electric field at that point over the 1000 ps time interval.

The results are also compared to an FDTD simulation employing Berenger's split field PML. The FDTD simulation is bound by the Courant, Friedrichs, and Lewy (CFL) limit

$$\Delta t \leq \Delta t_{\max} = \frac{1}{c\sqrt{\frac{1}{\Delta x^2}+\frac{1}{\Delta y^2}+\frac{1}{\Delta z^2}}} \tag{11}$$

where c is the speed of light within the host medium. Defining the ratio of $\Delta t/\Delta t_{\max}$ to be the CFL number (CFLN), the FDTD simulation is bound to a CFLN <1. Whereas, the ADI solution is not bound and can support a CFLN >1.

Fig. 1 illustrates the relative reflection error computed at point A as a function of time for the ADI method with different CFLN's, and for the FDTD method with a CFLN $= 1$ ($\Delta t = 1.926$ ps). In all cases, the PML parameters were scaled according to (9), with $\sigma_{s_{\max}} = \sigma_{opt}$ [(10)] and $m = 4$. Characteristically, the FDTD exhibits reflection errors that are small in the early time, and grow to a maximum asymptotic limit in the late time [3], [4], which is better than -80 dB. Interestingly, the ADI-PML exhibits its largest error in the early time and then relaxes to an asymptotic limit in the late time. It is also apparent that as the CFLN is increased, the reflection error increases.

Fig. 2 illustrates the maximum relative error at points A and point B as a function of the CFLN. As expected, the error at point A, which is predominately due to normally incident waves, is less than the error at point B. From Fig. 2, it is observed that when the CFLN $= 0.5$, the reflection error is the same level as the error realized by the FDTD terminated with Berenger's PML. However, increasing the CFLN increases the reflection error. To verify that this is not directly related to the choice of $\sigma_{s_{\max}}$ and m, a number of simulations were done to compute the error versus these parameters. As with the FDTD method, choosing $3 \leq m \leq 5$ is optimal and one sees little variance in the error within this range. Furthermore, even for larger CFLN's, choosing $\sigma_{s_{\max}} = \sigma_{opt}$ from (10) will give close to the minimum error. This is illustrated in Fig. 3.

IV. Conclusion

A 3-D alternating direction implicit (ADI) FDTD method employing the Berenger split-field PML equations was presented. It was found that the technique is unconditionally stable and supported time steps greater the CFL limit. Numerical example demonstrated that the ADI-PML does indeed provide wideband absorption of impinging electromagnetic waves. However, it was found that the reflection error increases when the CFL number is increased beyond one. In general, it was found that given a cubical spatial cell size of Δs, if $\lambda_{\min}/(\Delta s \cdot \text{CFLN}) > 25$, the ADI-PML method based on the split field-PML has good reflection properties. The one caveat is that the PML performance will degrade for low frequency excitations and long time exposures with the PML interface [3]. It is anticipated that this will ultimately be circumvented by alternative choices of constitutive parameters for the PML [6] as this technique continues to mature.

References

[1] F. Zheng, Z. Chen, and J. Zhang, "A finite–difference time-domain method without the courant stability conditions," *IEEE Microwave Guided Wave Lett.*, vol. 9, pp. 441–443, Nov. 1999.

[2] J. P. Berenger, "A perfectly matched layer for the absorption of electromagnetic waves," *J. Comput. Phys.*, vol. 114, pp. 185–200, Oct. 1994.

[3] ——, "Improved PML for the FDTD solution of wave-structure interaction problems," *IEEE Trans. Antennas Propagat.*, vol. 45, pp. 466–473, March 1997.

[4] S. D. Gedney, "Perfectly matched layer absorbing medium," in *Advances in Computational Electrodynamics: The Finite-Difference Time-Domain Method*, A. Taflove, Ed. Norwood, MA: Artech House, 1998, pp. 263–343.

[5] G. H. Golub and C. F. Van Loan, *Matrix Computations*, 2nd ed. Baltimore, MD: The Johns Hopkins Univ. Press, 1989.

[6] J. A. Roden and S. D. Gedney, "An efficient FDTD implementation of the PML with CFS in general media," in *2000 IEEE Int. Symp. Antennas and Propagation*, Salt Lake City, UT, July 16–21, 2000.